FEM formulation for analysis of soil constitutive model with a corner on the yield surface

Thirapong PIPATPONGSA*, Atsushi IIZUKA **, Ichizo KOBAYASHI*** and Hideki OHTA****

*Dept. of International Development Eng., Tokyo Institute of Technology, O-okayama, Meguro-ku, Tokyo 152-8550
** Dr. of Eng., Assoc. Prof., Dept. of Civil Eng., Kobe University, Rokkodai-cho, Nada-ku, Kobe 657-8501
*** Dr. of Eng., Research Associate, Dept. of Civil Eng., Tokyo Institute of Technology, O-okayama, Meguro-ku, Tokyo 152-8550
**** Dr. of Eng., Prof., Dept. of International Development Eng., ditto

Formulation and numerical implementation of soil constitutive model with a non-smooth elastic domain was developed based on Koiter's associated flow rule. The extension of standard FEM applicable to the model proposed by Sekiguchi and Ohta (1977) was made by adding a corner mode to assess plastic flow when a particular state of stress is placed at the corner. The extra implementation is added without any modification to the whole procedures of normal mode and general FEM codes. The comparisons between methods with/without a consideration of corner mode under K_o-condition were illustrated for both plane strain and axisymmetry. The effects of element assemblage and size of sub-incrementation were discussed. It was found that disregard of special treatment for the corner would produce unacceptable results in numerical analyses.

Key Words: finite element method, constitutive model, non-smooth yield surface

1. Introduction

Formulation and numerical implementation of soil constitutive models with a smooth/single yield surface have already been well developed and become a standard code for finite element method. Among many of engineering software and package, general FEM codes based on the soil constitutive model proposed by Sekiguchi and Ohta[1] (1977) have been extensively recognized in Japan and still being improved continuously. However, it has been found that a plastic flow at the point of preconsolidated stress, which is related to a material memory of the model, is unable to correctly evaluate plastic strain increments due to a problem of mathematical singularity on yield surface at which the gradient is not uniquely defined. A geometrical representation of the yield surface in stress space shows this point representing a ridge corner of asymmetrical logarithmic spiral. As a consequence, the discontinuous slope at the corner rules out the normality postulate; the similar difficulty in numerical implementation is also found by Britto & Gunn[2] (1987) and Gens & Potts[3] (1988) in original Cam-clay model[4] (Roscoe, Schofield & Thurairajah, 1963).

The discontinuity is suggested to be eliminated either by rounding off using smooth approximating functions (Zienkiewicz & Pande[5], 1977) or adopting an ellipsoidal yield surface (Roscoe & Burland[6], 1968). Actually, there is no theoretical objection to non-smooth yield surface (Koiter[7], 1953,

Rudnicki & Rice[8], 1975, Christoffersen & Hutchinson[9], 1979). Moreover, evaluation of plastic flow at the point of singularity can be achieved theoretically without any modification of a yield surface's curvature.

One of the theoretical extensions to cover constitutive models with the point of discontinuity, where elastic domain is defined by non-smooth convex boundaries, is developed by Simo, Kennedy & Govindjee[10] (1988), showing that the standard Kuhn-Tucker optimality conditions of convex mathematical programming are essentially equivalent to the multisurface counterpart of the conditions in Koiter (1953). By the abovementioned approach, Pipatpongsa et al.[11,12] (2001a, b) described an additional procedure to handle a difficulty when a particular stress point is placed at the corner of yield surface in stress space. Under this concept, K_o consolidation process is regulated by two activated yield loci referred to upper and lower yield surfaces intersecting each other in axisymmetric triaxial plane to form the hardening vertex, in which plastic flow at the point of discontinuity lie within the fan of possible directions.

The approach of adjoining the singular corner by only two conceivable yield functions can reduce bulky equations required by Koiter's condition for non-smooth multisurface plasticity. The coefficient of earth pressure at rest governed by the SO (Sekiguchi-Ohta) model can be obtained[13] by connecting a typical normality of individual yield surface to Koiter's

associated flow rule (Pipatpongsa et al., 2001c). The application of compatible Kuhn-Tucker optimality conditions and Koiter's flow rule to the model is illustrated by unconditionally stable return-mapping algorithm[14] (Pipatpongsa et al., 2001d).

In a view of practice, most of natural soil formation possesses a certain degree of over-consolidated ratio; therefore, an initial stress is placed inside a yield surface rather than at the corner. To avoid the same problem in normal consolidated young clay, an initial stress placed at the corner is put inside yield surface intentionally by factoring it with a number that is slightly less than one. Besides, a calculation of one-dimensional consolidation is obtained by assuming soil media as an elastic material. By means of those reasons, error due to the singularity is not exaggerated in finite element program applicable to the SO model, for example DACSAR (Iizuka & Ohta[15], 1987). However, in rigorous aspect, this fact cannot be overlooked and violated any longer.

In this paper, a standard FEM procedures based on smooth yield surface was corrected by adding a corner mode to assess plastic flow when stress is defined at the corner in particular. Detailed procedures with theoretical background are provided. A continuum tangential stiffness tensor corresponding to the singular corner of the SO model was formulated. The comparisons between methods with/without a consideration corner mode under K_o-condition were illustrated under plane strain and axisymmetric conditions. The effects of element assemblage and size of sub-incrementation were discussed. The study may provide a source of numerical implementation to fill in the overlooked procedure in previous development of FEM applicable to the SO or similar models.

2. Soil Constitutive Equations

The SO model has been proven to produce predicted behaviors which are consistent with observed field responses for anisotropically consolidated soils. The model is based on critical state theory considering dilatancy, reorientation of principal stresses, anisotropy and time dependency. The SO model is reduced to be the original Cam-clay model in case of initially isotropic stress condition.

2.1 Forms of the Sekiguchi-Ohta Model

The two-invariant, rate-independent elastoplastic associative soil constitutive model proposed by Sekiguchi and Ohta (1977) is originally expressed by a convex yield (plastic potential) function:

$$f(\sigma',h) \equiv f(p',\eta^*,\varepsilon_v^p) = MD\ln\left(\frac{p'}{p'_o}\right) + D\eta^* - \varepsilon_v^p = 0 \quad (2.1)$$

where σ' = effective stress tensor; h = selective isotropic hardening parameter; p' = effective mean stress; $\eta*$ = generalized stress ratio; ε_v^p = volumetric plastic strain; p'_o = effective mean stress at the end of completion of anisotropic consolidation (typically, K_o consolidation); M = slope of critical state line in a p'-q plane; D = coefficient of dilatancy. Internal variable h controls a size of a yield surface and can be selected either as stress-like or strain-like variable. A form in Eq.(2.1) serves as strain-like type, which physically means that a hardening/softening characteristics of material is induced by a plastic volumetric strain. On the other hand, a stress-like type can be formulated from Eq.(2.1) using relations given in Eqs.(2.2)-(2.3). Without loss of originality, an alternative form of the Sekiguchi-Ohta model with stress hardening as parameter can be expressed by Eq.(2.4)

$$p'_c = p'_o \exp\left(\frac{\varepsilon_v^p}{(\lambda-\kappa)/(1+e_o)}\right) \quad (2.2)$$

$$D = \frac{\lambda-\kappa}{M(1+e_o)} \quad (2.3)$$

$$f(\sigma',h) \equiv f(p',\eta^*,p'_c) = MD\ln\left(\frac{p'}{p'_c}\right) + D\eta^* = 0 \quad (2.4)$$

where p'_c = stress hardening parameter

2.2 Generalized Convex Format

For later reference throughout the paper, it is more convenient and general to rewrite the yield function of Eq.(2.4) in terms of stress invariants and joint invariant between stress tensor σ' and stress hardening tensor σ'_c which is kept along paths of corner as,

$$f(\sigma',\sigma'_c) = f(I_1,\bar{J}_2,I_{c1}) \quad \text{in which}$$

$$f(I_1,\bar{J}_2,I_{c1}) = MD\ln\left(\frac{I_1}{I_{c1}}\right) + D\frac{3\sqrt{3\bar{J}_2}}{I_1} = 0 \quad (2.5)$$

where, $I_1 = tr(\sigma') = 1:\sigma'$ $\quad (2.6)$

$$I_{c1} = tr(\sigma'_c) = 1:\sigma'_c \quad (2.7)$$

$$s = \sigma' - \frac{1}{3}I_1 1 = A:\sigma' \quad (2.8)$$

$$s_c = \sigma'_c - \frac{1}{3}I_{c1}1 = A:\sigma'_c \quad (2.9)$$

$$J_2 = \frac{1}{2}tr(s^2) = \frac{1}{2}s:s \quad (2.10)$$

$$J_{c2} = \frac{1}{2}tr(s_c^2) = \frac{1}{2}s_c:s_c \quad (2.11)$$

$$\eta_c = \frac{s_c}{p'_c} = \frac{s_o}{p'_o} = \eta_o \quad (2.12)$$

$$\bar{s} = s - \frac{1}{3}I_1\eta_c = \left(A - \frac{1}{3}\eta_c \otimes 1\right):\sigma' \quad (2.13)$$

-186-

$$\bar{J}_2 = \frac{1}{2} tr(\bar{\mathbf{s}}^2) = \frac{1}{2} \bar{\mathbf{s}} : \bar{\mathbf{s}} \tag{2.14}$$

The second-order identity tensor is defined by

$$\mathbf{1} \equiv \delta_{ij} \mathbf{e}_i \otimes \mathbf{e}_j \tag{2.15}$$

The identity forth-order tensor is defined by

$$\mathbf{I} \equiv \frac{1}{2} \big[\delta_{ik} \delta_{jl} + \delta_{il} \delta_{jk} \big] \mathbf{e}_i \otimes \mathbf{e}_j \otimes \mathbf{e}_k \otimes \mathbf{e}_l \tag{2.16}$$

The deviatoric forth-order tensor is defined by

$$\mathbf{A} \equiv \mathbf{I} - \frac{1}{3} (\mathbf{1} \otimes \mathbf{1}) \tag{2.17}$$

The notations of tensor and tensorial operation are shown in Appendix E. A schematization of reciprocal basic used in numerical implementation is supplemented in Appendix F.

2.3 Geometrical Representation

The SO yield surface in three principal stresses space can be conveniently presented by referring to a new Cartesian coordinate system (X_1, X_2, X_3) on the deviatoric plane (π-plane) as shown in Fig.1. The parametric form of yield surface on (p', ω) is formulated by coordinate transformation system (see, Appendix A). Fig.2 shows a distorted bullet shape of elastic domain in principal stress space and in different views on plane Ⓐ, Ⓑ and Ⓒ which refer to deviatoric plane, meridional plane at $\omega = 0$ and π, and top view (σ'_2- σ'_3) plane respectively. It is observed that there is a singular corner on the yield surface. Hence, the SO yield surface is not smooth at the particular stress point. This point is identified as the hardening vertex where material memory of consolidation history is kept as hardening parameter of the model.

3. Incremental Stress-Strain Relation

It is generally assumed that strain increment can be decomposed into elastic and plastic parts, denoted by

$$\dot{\boldsymbol{\varepsilon}} = \dot{\boldsymbol{\varepsilon}}^e + \dot{\boldsymbol{\varepsilon}}^p \tag{3.1}$$

Associated flow rule is applied to the SO model to determine irreversible plastic flow emerged in an outward normal direction to the plastic potential coincided with yield surface.

$$\dot{\boldsymbol{\varepsilon}}^p = \gamma \frac{\partial f}{\partial \boldsymbol{\sigma}'} = \gamma \partial_{\boldsymbol{\sigma}'} f \tag{3.2}$$

where γ is a proportional factor or consistency parameter Consequence of the consistency relation gives

$$\gamma = \frac{\partial_{\boldsymbol{\sigma}'} f : \mathbf{c}^e : \dot{\boldsymbol{\varepsilon}}}{H_e + H_p} \tag{3.3}$$

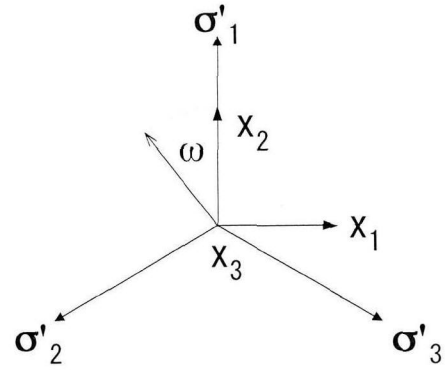Elastic tangential moduli $\mathbf{c}^e$, plastic moduli H_e and H_p are defined by,

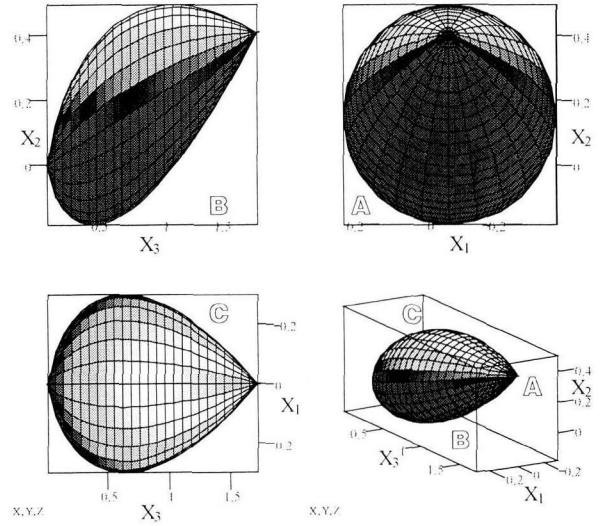Figure 1: Deviatoric plane in principal stress space where Cartesian coordinate is placed

Figure 2: Various views of the Sekiguchi-Ohta yield surface in principal stress space

$$\mathbf{c}^e = K\mathbf{1} \otimes \mathbf{1} + 2G\mathbf{A} \tag{3.4}$$

$$H_e = \partial_{\boldsymbol{\sigma}'} f : \mathbf{c}^e : \partial_{\boldsymbol{\sigma}'} f \tag{3.5}$$

$$H_p = -\frac{1 + e_o}{\lambda - \kappa} tr(\partial_{\boldsymbol{\sigma}'} f) p'_c \, \partial_{p'_c} f = tr(\partial_{\boldsymbol{\sigma}'} f) \tag{3.6}$$

e_o is a reference void ratio at a state of σ'_o. λ (=0.434C_c) and κ (=0.434C_s) are compression and swelling indices obtained from triaxial tests. Failure condition is defined when the plastic modulus H_p approaches zero. According to Eqs.(3.1)-(3.6), the incremental stress-strain relation can be formulated by

$$\dot{\boldsymbol{\sigma}}' = \mathbf{c}^e : (\dot{\boldsymbol{\varepsilon}} - \gamma \partial_{\boldsymbol{\sigma}'} f) = \left\{ \mathbf{c}^e - \frac{\mathbf{c}^e : \partial_{\boldsymbol{\sigma}'} f \otimes \partial_{\boldsymbol{\sigma}'} f : \mathbf{c}^e}{H_e + H_p} \right\} : \dot{\boldsymbol{\varepsilon}} \tag{3.7}$$

K and G are referred to bulk and shear moduli respectively. ν' is Poisson's ratio of soil skeleton. Dependence of K and G on p' suggests a hypo-elastic model is employed in a formulation.

$$K = \frac{p'}{\kappa} (1 + e_o) \tag{3.8}$$

$$G = \frac{3(1-2\nu')}{2(1+\nu')}K \qquad (3.9)$$

The first derivative of the SO model respective to stress tensor is shown in Appendix B. Substitution of these terms to Eq.(3.7) yields,

$$\frac{\mathbf{c}^e : \partial_{\sigma'}f \otimes \partial_{\sigma'}f : \mathbf{c}^e}{H_e + H_p} = \frac{\left(K\beta\mathbf{1} + \sqrt{6}G\overline{\mathbf{n}}\right) \otimes \left(K\beta\mathbf{1} + \sqrt{6}G\overline{\mathbf{n}}\right)}{K\beta^2 + 3G + \dfrac{I_1}{3D}\beta} \qquad (3.10)$$

where

$$\mathbf{c}^e : \partial_{\sigma'}f = 3\frac{D}{I_1}\left(K\beta\mathbf{1} + 2G\sqrt{\frac{3}{2}}\overline{\mathbf{n}}\right) \qquad (3.11)$$

$$H_e + H_p = \left(3\frac{D}{I_1}\right)^2\left(K\beta^2 + 3G\right) + 3\frac{D}{I_1}\beta \qquad (3.12)$$

$$\beta = M - 3\frac{\sqrt{3\overline{J}_2}}{I_1} - \sqrt{\frac{3}{2}}\left(\mathbf{\eta}_c : \overline{\mathbf{n}}\right) \qquad (3.13)$$

$$\eta_o = \frac{3(1-K_o)}{1+2K_o}, \quad \overline{\mathbf{n}} = \frac{\overline{\mathbf{s}}}{\|\mathbf{s}\|} = \frac{\overline{\mathbf{s}}}{\sqrt{2\overline{J}_2}} \qquad (3.14), (3.15)$$

$$\mathbf{\eta}_c = \sqrt{\frac{2}{3}}\eta_o\begin{bmatrix} -\dfrac{\sqrt{6}}{6} & 0 & 0 \\ 0 & \dfrac{\sqrt{6}}{3} & 0 \\ 0 & 0 & -\dfrac{\sqrt{6}}{6} \end{bmatrix} \qquad (3.16)$$

$\mathbf{\eta}_c$ is an aligned direction along hardening vertex in stress space.

4. Treatment of the Singular Corner

Since the stress state at the singular corner is referred the stress at triaxial condition[12], Fig.3 shows the yield loci and intersecting corner in the meridional plane associated to the triaxial stress plane (Rendulic's stress plane). The upper and lower yield loci are expressed as,

$$f_U(I_1, J_2, I_{c1}) = MD\ln\left(\frac{I_1}{I_{c1}}\right) + D\left(\frac{3\sqrt{3J_2}}{I_1} - \frac{3\sqrt{3J_{c2}}}{I_{c1}}\right) = 0$$

$$f_L(I_1, J_2, I_{c1}) = MD\ln\left(\frac{I_1}{I_{c1}}\right) - D\left(\frac{3\sqrt{3J_2}}{I_1} - \frac{3\sqrt{3J_{c2}}}{I_{c1}}\right) = 0$$

$$(4.1), (4.2)$$

Eq.(4.1) and its conjugate Eq.(4.2) are chosen as candidates among conceivable yield functions passing the corner. Since bulky equations are generated in corresponding to the number of non-smooth yield functions in concern, this approach gives the smallest forms needed by Koiter's condition. Concerning with Koiter's associated flow rule, plastic flow at the corner is interpreted as a resulting vector of plastic flow of upper and lower yield loci and expressed by,

$$\dot{\mathbf{\epsilon}}^P = \gamma_U\partial_{\sigma}f_U + \gamma_L\partial_{\sigma}f_L \qquad (4.3)$$

Incremental stress-strain relation is expressed by

$$\dot{\mathbf{\sigma}}' = \mathbf{c}^e : (\dot{\mathbf{\epsilon}} - \dot{\mathbf{\epsilon}}^P) \qquad (4.4)$$

According to App. D, substitute Eq.(D.9) into (4.3), obtain

$$\dot{\mathbf{\epsilon}}^P = \begin{pmatrix} \gamma_U \\ \gamma_L \end{pmatrix} \cdot \begin{pmatrix} \partial_{\sigma'}f_U \\ \partial_{\sigma'}f_L \end{pmatrix} = \mathbf{X}^{-1} \cdot \begin{pmatrix} \partial_{\sigma'}f_U : \mathbf{c}^e : \dot{\mathbf{\epsilon}} \\ \partial_{\sigma'}f_L : \mathbf{c}^e : \dot{\mathbf{\epsilon}} \end{pmatrix} \cdot \begin{pmatrix} \partial_{\sigma'}f_U \\ \partial_{\sigma'}f_L \end{pmatrix} \qquad (4.5)$$

Substitute Eq.(4.5) into (4.4) to obtain a stress increment,

$$\dot{\mathbf{\sigma}}' = \left(\mathbf{c}^e - \begin{pmatrix} \chi_{UU}\mathbf{g}_U \otimes \mathbf{g}_U + \chi_{UL}\mathbf{g}_U \otimes \mathbf{g}_L \\ + \chi_{LU}\mathbf{g}_L \otimes \mathbf{g}_U + \chi_{LL}\mathbf{g}_L \otimes \mathbf{g}_L \end{pmatrix}\right) : \dot{\mathbf{\epsilon}} \qquad (4.6)$$

where

$$\mathbf{g}_U = \mathbf{c}^e : \partial_{\sigma'}f_U = \frac{3D}{I_1}\left(K\left(M - 3\frac{\sqrt{3J_2}}{I_1}\right)\mathbf{1} + 2G\sqrt{\frac{3}{2}}\mathbf{n}\right) \qquad (4.7)$$

$$\mathbf{g}_L = \mathbf{c}^e : \partial_{\sigma'}f_L = \frac{3D}{I_1}\left(K\left(M + 3\frac{\sqrt{3J_2}}{I_1}\right)\mathbf{1} - 2G\sqrt{\frac{3}{2}}\mathbf{n}\right) \qquad (4.8)$$

$\chi = \mathbf{X}^{-1}$ is defined in a way that,

$$\chi_{UU} = \chi_{1,1}; \chi_{UL} = \chi_{1,2}; \chi_{LU} = \chi_{2,1}; \chi_{LL} = \chi_{2,2} \qquad (4.9)$$

According to Appendices C and D, coupled hardening matrix is expressed by Eq.(4.10) as,

$$\mathbf{X} = \left(3\frac{D}{I_1}\right)^2\begin{bmatrix} K\beta_U^2 + 3G + \dfrac{I_1}{3D}\beta_U & K\beta_U\beta_L - 3G + \dfrac{I_1}{3D}\beta_L \\ K\beta_L\beta_U - 3G + \dfrac{I_1}{3D}\beta_U & K\beta_L^2 + 3G + \dfrac{I_1}{3D}\beta_L \end{bmatrix}$$
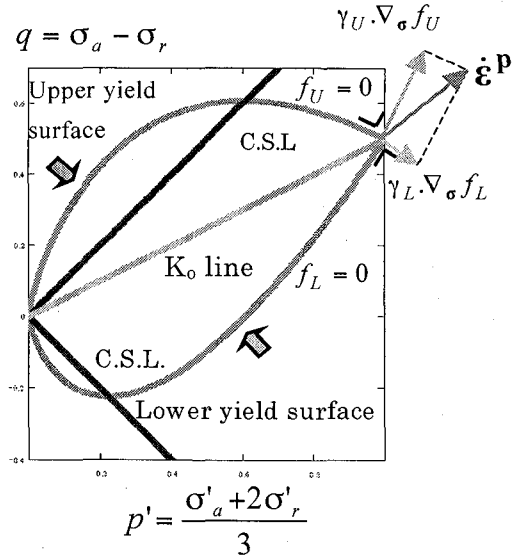
$$(4.10)$$

Figure 3: p'-q plane in the meridional section is associated to the triaxial stress plane where the corner is placed

Eq.(4.6) reveals a incremental stress-strain relations in Eq.(4.11).

$$\dot{\sigma}' = \mathbf{c}^{ep} : \dot{\varepsilon} \qquad (4.11)$$

A formulation of tangential elastoplastic moduli considering corner mode is generally expressed by Eq.(4.12) as,

$$\mathbf{c}^{ep} = \mathbf{c}^{e} - \sum_{\alpha,\beta \in \{U,L\}} \chi_{\alpha,\beta}\left(\mathbf{g}_{\alpha} \otimes \mathbf{g}_{\beta}\right) \qquad (4.12)$$

5. FEM Formulation

Four-node displacement-based element with 2x2 Gauss integration is formulated by standard FEM methodology for both plane strain and axisymmetric conditions. A procedure for corner mode is added to normal mode by employing tangential elastoplastic moduli defined in Eq.(4.11). A corner mode is judged to activate by extra condition given in Eq. (5.1). If the condition is invalid then a computation is handled by a general mode, which simply means stress is located out of the corner. A condition for elastic unloading is defined in Eq.(5.2).

$$f_U \geq ZERO \quad \text{and} \quad f_L \geq ZERO \qquad (5.1)$$

$$L_U < ZERO \quad \text{and} \quad L_L < ZERO \qquad (5.2)$$

where ZERO is a zero truncation allowed in computation, usually set to a very small positive number, e.g. 10^{-12}

FEM simulations of K_o-condition can be performed by considering one-quarter of specimen enclosed by stiff lateral boundary depicted by Fig.4. Type A model refers to a true K_o condition controlled by zero lateral strain while type B refers to a reversed K_o condition controlled by a lateral pressure generated by K_o value. Geometric boundary conditions are shown in Fig.5 showing both single and four-element assemblage denoted by numerator 1 and 2 respectively. Material parameters with initial conditions for a class of inviscid SO model are listed in Table 1. Code names of all cases are tabulated in Table 2. Symbols + and - notify a calculation performed with or without corner mode. Applied vertical load of σ'_{vo} (100 kN/m^2) is further subdivided into 100 sub-steps for all cases except two latest cases where 1000 and 5000 sub-steps are applied to observe sizes of sub-steps affected in computations.

Table 1: Soil parameters

Parameter	Description	Value
D	Coefficient of dilatancy	0.101
Λ	Irreversibility ratio	0.825
M	Critical state parameter	1.120
v'	Effective Poisson's ratio	0.364
K_o	Coefficient of earth pressure (NC)	0.572
K_i	Coefficient of earth pressure (in-situ)	0.572
λ	Compression index	0.342
e_o	Void ratio at σ'_{vo}	1.500
σ'_{vo}	Eff. preconsolidation pressure (kN/m^2)	100
σ'_{vi}	Eff. overburden pressure (kN/m^2)	100

6. Calculation Results

Results of effective stresses, shear stress and ratio of horizontal stress to vertical stress were listed in Table 3. Strains and ratio of deviatoric strain to volumetric strain were shown in Table 4. Isotropic hardening stress, volumetric and deviatoric plastic strain, ratio of deviatoric to volumetric plastic strain and ratio of volumetric plastic strain to volumetric strain were shown in Table 5. Results in Tables 3-5 indicate that, under K_o-condition, FEM procedures with/without corner mode give a substantially different results. The exact solutions given in Eqs.(6.1)-(6.4) are obtained from a basic 1-D consolidation problem. Therefore, cases of A1a+, A1p+, B1p+, A2a+, A2p+ and B2p+ are equivalent one another and provide the reasonable results. Calculations without corner mode failed to give reasonable results.

$$\sigma'_{y(z)} = \sigma'_{oy(z)} + \Delta\sigma'_{y(z)}, \quad \sigma'_{x(r)} = \sigma'_{z(\theta)} = K_o\sigma'_{y(z)} \qquad (6.1)$$

$$\tau_{xy(rz)} = 0, \quad p'_c = \frac{1}{3}\sigma'_{y(z)}(1+2K_o) \qquad (6.2)$$

$$\varepsilon_{y(z)} = \frac{\lambda}{1+e_o}\ln\left(\frac{\sigma'_{y(z)}}{\sigma'_{oy(z)}}\right), \quad \varepsilon_{x(r)} = \varepsilon_{z(\theta)} = 0 \qquad (6.3)$$

$$\frac{\varepsilon_s}{\varepsilon_v} = \frac{\varepsilon_s^p}{\varepsilon_v^p} = \frac{2}{3}, \quad \frac{\varepsilon_v^p}{\varepsilon_v} = \Lambda \qquad (6.4)$$

It is found that results obtained by single element (for A1a+, A1p+, B1p+) and four-element (for A2a+, A2p+, B2p+) generate almost same responses due to a class of homogeneous deformation. There is no effect of subdivision of spatial domain in the calculation, but there is an effect of subdivision of time domain (sub-incrementation of loading) as illustrated by results obtained from case A1a+* and A1a+**, that is, a more exact result can be taken for a finer sub-step. Herein, 5000 sub-steps are required to yield an exact solution. Type B model gave correct responses only for plane strain condition. Therefore, a restraint in plane strain condition is satisfied for a reversed or stress-controlled K_o-condition where stress path is kept along the corner. A comparison between A1a+ and A1a- alone are shown in Figs.6-9. It is clearly found that without corner mode, stress paths are mobilized along K_o-line, resulting in fluctuated paths in Fig.6. Volumetric contraction given by cases without corner mode is less than a solution (see, Figs.7 and 8). Moreover, the slope of e-log(σ'_v) curve (see, Fig.9) is not equal to the compression index (in log$_{10}$-scale) C_c while a procedure with corner mode can produce responses associated to the solution.

7. Conclusion

FEM procedures including a corner mode were formulated using Koiter's associated flow rule to evaluate plastic flow and derive for incremental stress-strain relation at the hardening vertex of the SO yield surface in meridional plane under K_o-condition.
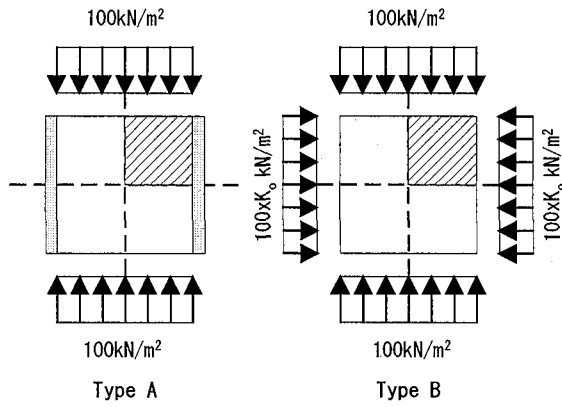
Figure 4: K_o condition (type A) and reversed K_o condition given by applying a lateral pressure generated by K_o value (type B)
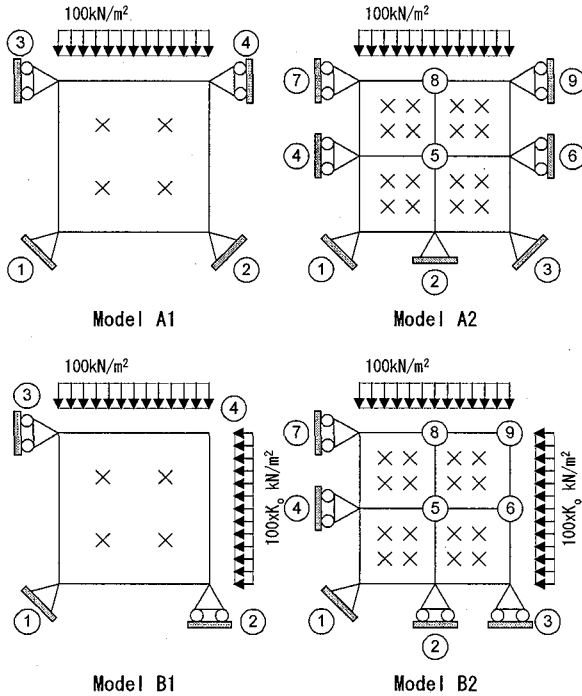

Figure 5: Schematic description of single element and four-element assemblage

Table 2: Case study classification (100 sub-steps)

Code	Geometry/Elements	Corner effect
A1a+	axisymmetric/A1	considered
A1a-	axisymmetric/A1	ignored
A1p+	plane strain/A1	considered
A1p-	plane strain/A1	ignored
B1a+	axisymmetric/B1	considered
B1a-	axisymmetric/B1	ignored
B1p+	plane strain/B1	considered
B1p-	plane strain/B1	ignored
A2a+	axisymmetric/A2	considered
A2p+	plane strain/A2	considered
B2a+	axisymmetric/B2	considered
B2p+	plane strain/B2	considered
A1a+*	A1a+ by 1000 sub-steps	
A1a+**	A1a+ by 5000 sub-steps	

Table 3: Calculation results: effective stress (kN/m²)

Case	$\sigma'_{x(r)}$	$\sigma'_{y(z)}$	$\tau_{xy(rz)}$	$\sigma'_{z(\theta)}$	$\sigma'_{x(r)}/\sigma'_{y(z)}$
A1a+	114.50	200	0	114.50	0.572
A1a-	114.98	200	0	114.98	0.575
A1p+	114.50	200	0	114.50	0.572
A1p-	114.98	200	0	114.98	0.575
B1a+	113.75	198.13	-9.08E-5	113.75	0.572
B1a-	114.50	200	0	114.50	0.572
B1p+	114.50	200	0	114.50	0.572
B1p-	114.50	200	0	114.35	0.572
A2a+	114.50	200	0	114.50	0.572
A2p+	114.50	200	0	114.50	0.572
B2a+	113.80	199.50	0.03	113.55	0.570
B2p+	114.50	200	0	114.50	0.572
A1a+*	114.50	200	0	114.50	0.572
A1a+**	114.50	200	0	114.50	0.572
Exact	114.50	200	0	114.50	0.572

Table 4: Calculation results: strain

Case	$\varepsilon_{x(r)}$	$\varepsilon_{y(z)}$	$\gamma_{xy(rz)}$	$\varepsilon_{z(\theta)}$	$\varepsilon_s/\varepsilon_v$
A1a+	0	0.094	0	0	0.667
A1a-	0	0.030	0	0	0.667
A1p+	0	0.094	0	0	0.667
A1p-	0	0.030	0	0	0.667
B1a+	0.025	0.043	1.21E-3	0.025	0.137
B1a-	5.89E-3	0.022	0	5.89E-3	0.323
B1p+	0	0.094	0	0	0.667
B1p-	7.28E-3	0.025	0	0	0.462
A2a+	0	0.094	0	0	0.667
A2p+	0	0.094	0	0	0.667
B2a+	0.020	0.046	9.27E-4	0.019	0.208
B2p+	0	0.094	0	0	0.667
A1a+*	0	0.095	0	0	0.667
A1a+**	0	0.095	0	0	0.667
Exact	0	0.095	0	0	0.667

Table 5: Calculation results: plastic variables

Case	p'_c	ε_v^p	ε_s^p	$\varepsilon_s^p/\varepsilon_v^p$	$\varepsilon_v^p/\varepsilon_v$
A1a+	142.28	0.077	0.052	0.667	0.823
A1a-	143.84	0.014	9.24E-3	0.683	0.448
A1p+	142.28	0.077	0.052	0.667	0.823
A1p-	143.84	0.014	9.24E-3	0.683	0.448
B1a+	141.57	0.076	2.13E-3	0.028	0.823
B1a-	142.28	0.018	0.000	0.000	0.515
B1p+	142.28	0.077	0.052	0.667	0.823
B1p-	142.69	0.016	5.42E-3	0.339	0.491
A2a+	142.28	0.077	0.052	0.667	0.823
A2p+	142.28	0.077	0.052	0.667	0.823
B2a+	142.45	0.069	6.67E-3	0.097	0.807
B2p+	142.28	0.077	0.052	0.667	0.823
A1a+*	142.93	0.078	0.052	0.667	0.825
A1a+**	142.98	0.078	0.052	0.667	0.825
Exact	143.00	0.078	0.052	0.667	0.825

The extra implementation is added without any modification to the whole procedures of a normal mode and general FEM codes. Disregard of special treatment for the corner would produce unacceptable results.
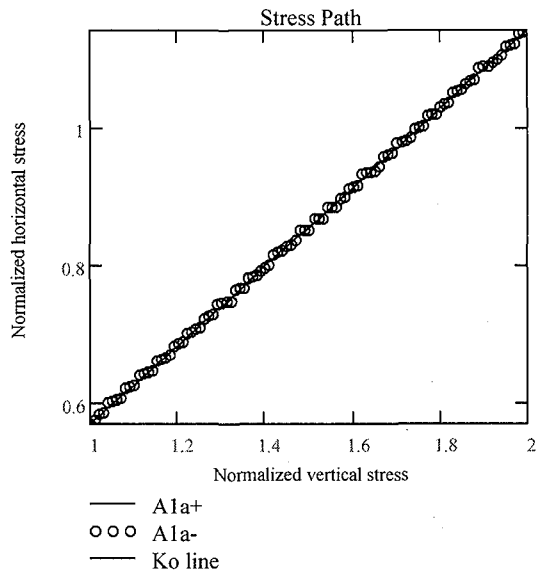
Stress Path

A1a+
o o o A1a-
── Ko line

Figure 6: Normalized stress paths of vertical and horizontal stresses

Stress-Strain Curve

A1a+
o o o A1a-
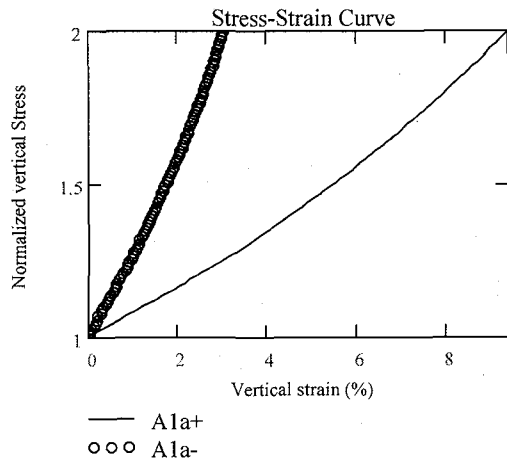
Figure 7: Normalized vertical stress-vertical strain curves

Strain Path

A1a+
o o o A1a-
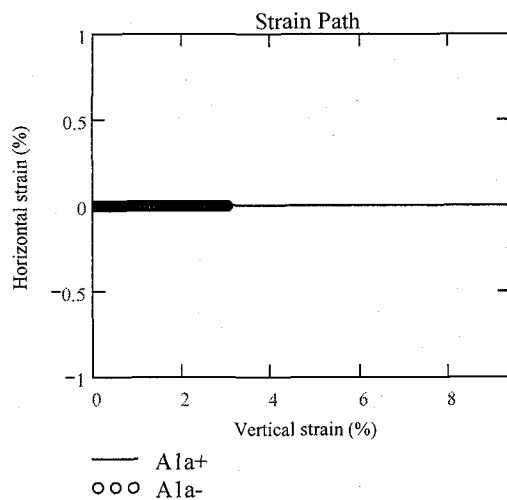
Figure 8: Strain paths of vertical and horizontal strains

e-log(vertical stress) curve
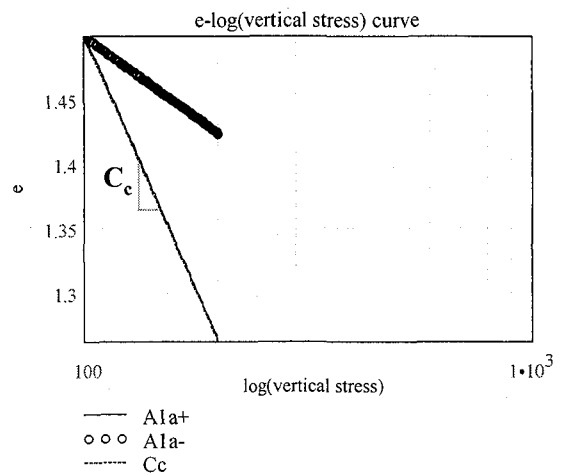

── A1a+
o o o A1a-
------- Cc

Figure 9: e-log(σ'_v) curve under compression loading

It is clearly seen that a corner mode is considerably needed especially for a particular type of problems such as analysis of K_o consolidation, self-weight consolidation, K_o creep and ageing as well as site responses when a level of water table is changed.

Appendices

A: Cartesian coordinate system in principal stress space

Relation between Cartesian coordinate system in principal stress space is expressed by using transformation tensor Q.

$$\mathbf{x} = \mathbf{Q} \cdot \mathbf{\sigma'} \tag{A.1}$$

where
$$\mathbf{Q} = \begin{bmatrix} 0 & \frac{-1}{\sqrt{2}} & \frac{1}{\sqrt{2}} \\ \sqrt{\frac{2}{3}} & \frac{-1}{\sqrt{6}} & \frac{-1}{\sqrt{6}} \\ \frac{1}{\sqrt{3}} & \frac{1}{\sqrt{3}} & \frac{1}{\sqrt{3}} \end{bmatrix}, \quad \mathbf{\sigma'} = \begin{pmatrix} \sigma'_1 \\ \sigma'_2 \\ \sigma'_3 \end{pmatrix}, \quad \mathbf{x} = \begin{pmatrix} x_1 \\ x_2 \\ x_3 \end{pmatrix}$$

x_3-axis is coincided with hydrostatic pressure axis and the principal mean stress is marked by,

$$x_3 = \sqrt{3} p' \tag{A.2}$$

Substitute Eq.(A.2) to Eq.(A.1) and solve for the arbitrary stress,

$$\mathbf{\sigma'} = \mathbf{Q}^T \cdot \mathbf{x} \tag{A.3}$$

The locus of yield surface intersecting with a constant mean stress can be obtained by substituting Eq.(A.3) to the yield function. Consequently, Eq.(2.4) yields,

$$f(\mathbf{\sigma'}, p'_c) = MD \ln\left(\frac{p'}{p'_c}\right) + D\sqrt{\frac{3x_2^2 - 2\sqrt{6}x_2\eta_o p' + 2\eta_o^2 p'^2 + 3x_1^2}{p'^2}} = 0 \tag{A.5}$$

Rearrange Eq.(A.5) to a particular expression below

$$x_1^2 + \left(x_2 - \frac{2}{\sqrt{6}}\eta_o p'\right)^2 = \left(\frac{2M}{\sqrt{6}}\ln\left(\frac{p'}{p'_c}\right)p'\right)^2 \qquad (A.6)$$

Transform Eq.(A.6) to polar coordinate system by introducing

$$R = \frac{2M}{\sqrt{6}}\ln\left(\frac{p'}{p'_c}\right)p', \qquad (A.7)$$

$$x_1 = R\sin\omega, \qquad x_2 = R\cos\omega + \frac{2}{\sqrt{6}}\eta_o p' \qquad (A.8, A.9)$$

where $\omega \in [0, 2\pi]$, $p' \in (0, p'_c]$

B: First derivatives of the Sekiguchi-Ohta yield function respective to stress tensor

By chain rule, the derivative can be written in terms of stress invariants

$$\partial_{\boldsymbol{\sigma}'}f = \partial_{I_1}f\partial_{\boldsymbol{\sigma}'}I_1 + \partial_{\bar{J}_2}f\partial_{\bar{s}}\bar{J}_2 : \partial_{\boldsymbol{\sigma}'}\bar{\mathbf{s}} \qquad (B.1)$$

$$\partial_{\boldsymbol{\sigma}'}I_1 = 1, \quad \partial_{\bar{s}}\bar{J}_2 : \partial_{\boldsymbol{\sigma}'}\bar{\mathbf{s}} = \left(\mathbf{A} - \frac{1}{3}\mathbf{1}\otimes\boldsymbol{\eta}_c\right):\bar{\mathbf{s}} \qquad (B.2, B.3)$$

Substitute Eqs.(B.2) and (B.3) into (B.1), obtain,

$$\partial_{\boldsymbol{\sigma}'}f = \left(\partial_{I_1}f - \sqrt{2\bar{J}_2}\partial_{\bar{J}_2}f\frac{1}{3}(\boldsymbol{\eta}_c : \bar{\mathbf{n}})\right)\mathbf{1} + \sqrt{2\bar{J}_2}\partial_{\bar{J}_2}f\bar{\mathbf{n}} \quad (B.4)$$

where

$$\partial_{I_1}f = \frac{D}{I_1}\left(M - 3\frac{\sqrt{3\bar{J}_2}}{I_1}\right) \qquad (B.5)$$

$$\sqrt{2\bar{J}_2}\partial_{\bar{J}_2}f = \sqrt{\frac{3}{2}}\frac{3D}{I_1} \qquad (B.6)$$

C: First derivatives of the upper and lower yield loci respective to stress tensor

By the similar fashion with App. B, the derivatives of upper and lower yield loci are expressed by

$$\partial_{\boldsymbol{\sigma}'}f_U = \partial_{I_1}f_U\mathbf{1} + \partial_{J_2}f_U\mathbf{s} = \partial_{I_1}f_U\mathbf{1} + \sqrt{2J_2}\partial_{J_2}f_U\mathbf{n} \quad (C.1)$$

$$\partial_{\boldsymbol{\sigma}'}f_L = \partial_{I_1}f_L\mathbf{1} + \partial_{J_2}f_L\mathbf{s} = \partial_{I_1}f_L\mathbf{1} + \sqrt{2J_2}\partial_{J_2}f_L\mathbf{n} \quad (C.2)$$

where

$$\partial_{I_1}f_U = \frac{D}{I_1}\left(M - 3\frac{\sqrt{3J_2}}{I_1}\right), \sqrt{2J_2}\partial_{J_2}f_U = \sqrt{\frac{3}{2}}\frac{3D}{I_1} \quad (C.3), (C.4)$$

$$\partial_{I_1}f_L = \frac{D}{I_1}\left(M + 3\frac{\sqrt{3J_2}}{I_1}\right), \sqrt{2J_2}\partial_{J_2}f_L = -\sqrt{\frac{3}{2}}\frac{3D}{I_1} \quad (C.5), (C.6)$$

$$\mathbf{n} = \frac{\mathbf{s}}{\sqrt{\mathbf{s}:\mathbf{s}}} = \frac{\mathbf{s}}{\sqrt{2J_2}} \qquad (C.7)$$

D: Consistency parameters of the upper and lower yield loci

Consistency parameters are determined from consistency condition subjected on both upper and lower yield loci to ensure both loci are active and activated under loading condition. Equate time derivatives of both upper and lower yield loci to zero and evaluate consistency parameters γ_U and γ_L.

$$\dot{f}_U = \partial_{\boldsymbol{\sigma}'}f_U : \dot{\boldsymbol{\sigma}}' + \partial_{p'_c}f_U\dot{p}'_c = 0 \qquad (D.1)$$

$$\dot{f}_L = \partial_{\boldsymbol{\sigma}'}f_L : \dot{\boldsymbol{\sigma}}' + \partial_{p'_c}f_L\dot{p}'_c = 0 \qquad (D.2)$$

The evolution law of isotropic stress hardening parameter is

$$\dot{p}'_c = \frac{p'_c}{MD}\dot{\varepsilon}_v^p \qquad (D.3)$$

The derivatives of upper and lower yield loci respective to p'_c are shown by

$$\partial_{p'_c}f_U = \partial_{p'_c}f_L = -\frac{MD}{p'_c} \qquad (D.4)$$

Substitute Eqs.(D.3) and (D.4) into (D.1) and (D.2), obtain

$$\dot{f}_U = \partial_{\boldsymbol{\sigma}'}f_U : \mathbf{c}^e : \left(\dot{\boldsymbol{\varepsilon}} - \dot{\boldsymbol{\varepsilon}}^p\right) + \partial_{p'_c}f_U\frac{p'_c}{MD}\dot{\boldsymbol{\varepsilon}}^p : 1 = 0 \quad (D.5)$$

$$\dot{f}_L = \partial_{\boldsymbol{\sigma}'}f_L : \mathbf{c}^e : \left(\dot{\boldsymbol{\varepsilon}} - \dot{\boldsymbol{\varepsilon}}^p\right) + \partial_{p'_c}f_L\frac{p'_c}{MD}\dot{\boldsymbol{\varepsilon}}^p : 1 = 0 \quad (D.6)$$

Rewrite Eqs.(D.1) and (D.2) by substituting Koiter's associated flow rule Eq.(4.3) into Eqs.(D.5) and (D.6), obtain

$$\gamma_U\left(H_{UU}^e + H_U^p\right) + \gamma_L\left(H_{UL}^e + H_L^p\right) = L_U \qquad (D.7)$$

$$\gamma_U\left(H_{LU}^e + H_U^p\right) + \gamma_L\left(H_{LL}^e + H_L^p\right) = L_L \qquad (D.8)$$

where $L_U = \partial_{\boldsymbol{\sigma}'}f_U : \mathbf{c}^e : \dot{\boldsymbol{\varepsilon}}$, $L_L = \partial_{\boldsymbol{\sigma}'}f_L : \mathbf{c}^e : \dot{\boldsymbol{\varepsilon}}$

$$H_{UU}^e = \partial_{\boldsymbol{\sigma}'}f_U : \mathbf{c}^e : \partial_{\boldsymbol{\sigma}'}f_U, \quad H_{UL}^e = \partial_{\boldsymbol{\sigma}'}f_U : \mathbf{c}^e : \partial_{\boldsymbol{\sigma}'}f_L$$

$$H_{LU}^e = \partial_{\boldsymbol{\sigma}'}f_L : \mathbf{c}^e : \partial_{\boldsymbol{\sigma}'}f_U, \quad H_{LL}^e = \partial_{\boldsymbol{\sigma}'}f_L : \mathbf{c}^e : \partial_{\boldsymbol{\sigma}'}f_L$$

$$H_U^p = tr\left(\partial_{\boldsymbol{\sigma}'}f_U\right), \quad H_L^p = tr\left(\partial_{\boldsymbol{\sigma}'}f_L\right)$$

Formulate Eqs.(D.7) and (D.8) to linear algebraic system and solved for consistency parameters

$$\begin{pmatrix}\gamma_U \\ \gamma_L\end{pmatrix} = \mathbf{X}^{-1} \cdot \begin{pmatrix}L_U \\ L_L\end{pmatrix} \qquad (D.9)$$

where $\mathbf{X} = \begin{bmatrix} H_{UU}^e + H_U^p & H_{UL}^e + H_L^p \\ H_{LU}^e + H_U^p & H_{LL}^e + H_L^p \end{bmatrix}$ (D.10)

$$H_U^p = 3\frac{D}{I_1}\beta_U, \quad H_L^p = 3\frac{D}{I_1}\beta_L \qquad (D.11), (D.12)$$

$$\beta_U = M - 3\frac{\sqrt{3J_2}}{I_1}, \quad \beta_L = M + 3\frac{\sqrt{3J_2}}{I_1} \qquad (D.13), (D.14)$$

$$H^e_{UU} = \left(\frac{3D}{I_1}\right)^2 \left(K\beta_U^2 + 3G\right) \tag{D.15}$$

$$H^e_{UL} = \left(3\frac{D}{I_1}\right)^2 \left(K\beta_U\beta_L - 3G\right) \tag{D.16}$$

$$H^e_{LU} = \left(3\frac{D}{I_1}\right)^2 \left(K\beta_L\beta_U - 3G\right) \tag{D.17}$$

$$H^e_{LL} = \left(\frac{3D}{I_1}\right)^2 \left(K\beta_L^2 + 3G\right) \tag{D.18}$$

E: Notations of tensor and tensorial operation

Standard notation is used throughout. Boldface symbols denote tensors. Italic symbols denote scalar components. A second-order tensor on Euclidean space $\mathbb{E}$ in respect to an orthonormal basic $\{\mathbf{e}_i\}$ are shown by,

$$\mathbf{T} = T_{ij}\mathbf{e}_i \otimes \mathbf{e}_j \tag{E.1}$$

Dot and double dots are used to indicate simple and double product (contraction) defined as following,

$$\begin{aligned}
\mathbf{T} \cdot \mathbf{D} &= T_{ij}D_{kl}\left(\mathbf{e}_i \otimes \mathbf{e}_j\right) \cdot \left(\mathbf{e}_k \otimes \mathbf{e}_l\right) \\
&= T_{ij}D_{kl}\left(\mathbf{e}_i \otimes \mathbf{e}_l\right)\left(\mathbf{e}_j \cdot \mathbf{e}_k\right) \\
&= T_{ik}D_{kl}\left(\mathbf{e}_i \otimes \mathbf{e}_l\right)
\end{aligned} \tag{E.2}$$

$$\begin{aligned}
\mathbf{T} : \mathbf{D} &= T_{ij}D_{kl}\left(\mathbf{e}_i \otimes \mathbf{e}_j\right) : \left(\mathbf{e}_k \otimes \mathbf{e}_l\right) \\
&= T_{ij}D_{kl}\left(\mathbf{e}_i \cdot \mathbf{e}_k\right)\left(\mathbf{e}_j \cdot \mathbf{e}_l\right) \\
&= T_{ij}D_{ij}
\end{aligned} \tag{E.3}$$

A double product of forth-order tensor and second-order tensor is expressed by,

$$\begin{aligned}
\mathbf{C} : \mathbf{D} &= C_{ijkl}\mathbf{e}_i \otimes \mathbf{e}_j \otimes \mathbf{e}_k \otimes \mathbf{e}_l : D_{mn}\mathbf{e}_m \otimes \mathbf{e}_n \\
&= C_{ijkl}\mathbf{e}_i \otimes \mathbf{e}_j \left(\mathbf{e}_k \cdot \mathbf{e}_m\right)\left(\mathbf{e}_l \cdot \mathbf{e}_n\right)D_{mn} \\
&= C_{ijkl}D_{kl}\mathbf{e}_i \otimes \mathbf{e}_j
\end{aligned} \tag{E.4}$$

A component of double product of forth-order tensor and forth-order tensor is expressed by,

$$\left(\mathbf{C} : \mathbf{E}\right)_{ijkl} = C_{ijmn}E_{mnkl} \tag{E.5}$$

A double product of forth-order tensor $\mathbf{C}$ and its inversion gives an identity forth-order tensor shown by,

$$\mathbf{C}^{-1} : \mathbf{C} = \mathbf{C} : \mathbf{C}^{-1} = \mathbf{I} \tag{E.6}$$

A double product of identity forth-order tensor $\mathbf{I}$ and second-order tensor results in a symmetric projection of that second-order tensor as,

$$\begin{aligned}
\mathbf{I} : \mathbf{T} &= \frac{1}{2}\left[\delta_{ik}\delta_{jl} + \delta_{il}\delta_{jk}\right]\mathbf{e}_i \otimes \mathbf{e}_j \otimes \mathbf{e}_k \otimes \mathbf{e}_l : T_{mn}\mathbf{e}_m \otimes \mathbf{e}_n \\
&= T_{mn}\frac{1}{2}\left[\delta_{ik}\delta_{jl} + \delta_{il}\delta_{jk}\right]\mathbf{e}_i \otimes \mathbf{e}_j \left(\mathbf{e}_k \cdot \mathbf{e}_m\right)\left(\mathbf{e}_l \cdot \mathbf{e}_n\right) \\
&= T_{mn}\frac{1}{2}\left[\delta_{ik}\delta_{jl} + \delta_{il}\delta_{jk}\right]\mathbf{e}_i \otimes \mathbf{e}_j \delta_{km}\delta_{ln} \\
&= T_{kl}\frac{1}{2}\left[\delta_{ik}\delta_{jl} + \delta_{il}\delta_{jk}\right]\mathbf{e}_i \otimes \mathbf{e}_j \\
&= \frac{1}{2}\left[T_{ij} + T_{ji}\right]\mathbf{e}_i \otimes \mathbf{e}_j
\end{aligned} \tag{E.7}$$

A forth-order tensor mapping stress and stress deviator is defined herein as deviatoric forth-order tensor $\mathbf{A}$. The derivation is shown below,

$$\mathbf{s} = \boldsymbol{\sigma} - \frac{1}{3}(\mathbf{1}:\boldsymbol{\sigma})\mathbf{1} = \left[\mathbf{I} - \frac{1}{3}\mathbf{1}\otimes\mathbf{1}\right]:\boldsymbol{\sigma} = \mathbf{A}:\boldsymbol{\sigma} \tag{E.8}$$

Symmetry is preserved for deviatoric forth-order tensor $\mathbf{A}$ as,

$$\mathbf{A}^T = \mathbf{I}^T - \frac{1}{3}(\mathbf{1}\otimes\mathbf{1})^T = \mathbf{I} - \frac{1}{3}(\mathbf{1}\otimes\mathbf{1}) = \mathbf{A} \tag{E.9}$$

A double product of deviatoric forth-order tensor $\mathbf{A}$ and isotropic second-order tensor is zero tensor.

$$\mathbf{A}:\mathbf{1} = \mathbf{I}:\mathbf{1} - \frac{1}{3}(\mathbf{1}\otimes\mathbf{1}):\mathbf{1} = \mathbf{1} - \frac{1}{3}(3)\mathbf{1} = \mathbf{0} \tag{E.10}$$

A double product of deviatoric forth-order tensor $\mathbf{A}$ and stress deviator $\mathbf{s}$ is a mapping to itself $\mathbf{s}$,

$$\mathbf{A}:\mathbf{s} = \mathbf{I}:\mathbf{s} - \frac{1}{3}(\mathbf{1}\otimes\mathbf{1}):\mathbf{s} = \mathbf{s} - \frac{1}{3}(0)\mathbf{1} = \mathbf{s} \tag{E.11}$$

F: Schematization of reciprocal basic

Apart from the tensor basis $\mathbf{e}_i \otimes \mathbf{e}_j$, which is independent of any preferred choice of basic for $\mathbb{E}$, there is an additional linear mapping $\boldsymbol{\eta}_c$ set in space to characterize material anisotropy in particular. A resulting reciprocal basis considering a relative relation between Cartesian and anisotropic mapping quantity is schematized in Fig.10 and Fig.11 and also written in expressions given below,

$$\boldsymbol{\sigma}' = p'\mathbf{1} + p'\boldsymbol{\eta}_c + \overline{\mathbf{s}} \tag{F.1}$$

$$\boldsymbol{\sigma}'_c = p'_c\mathbf{1} + p'_c\boldsymbol{\eta}_c \tag{F.2}$$

Relative stress deviator $\overline{\mathbf{s}}$ in Eq.(F.3) is coaxial with deviatoric plastic flow; thus, it is more suitable than stress deviator $\mathbf{s}$ in the manipulation of anisotropic constitutive equations.

$$\overline{\mathbf{s}} = \mathbf{s} - p'\boldsymbol{\eta}_c = \sqrt{2\overline{J}_2}\,\overline{\mathbf{n}} \tag{F.3}$$

As a result, a stress tensor can be represented in terms of reciprocal tensor bases $\{\mathbf{1}, \boldsymbol{\eta}_c, \overline{\mathbf{n}}\}$.
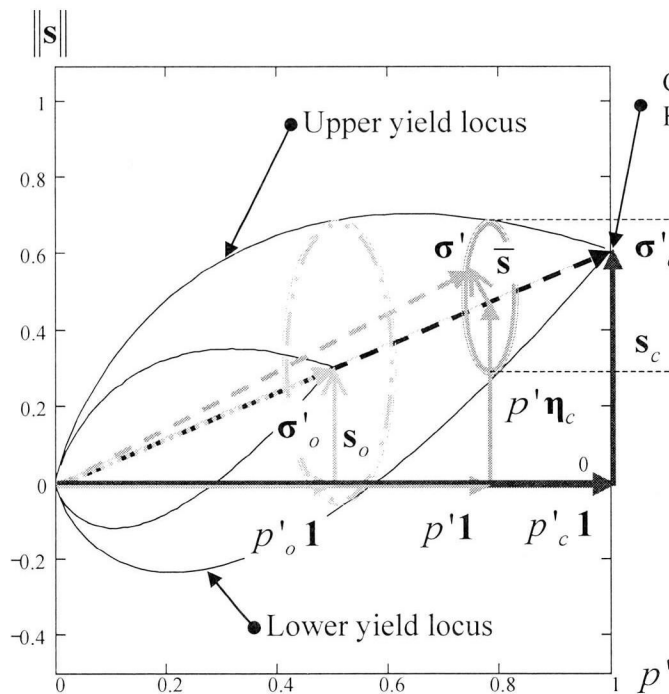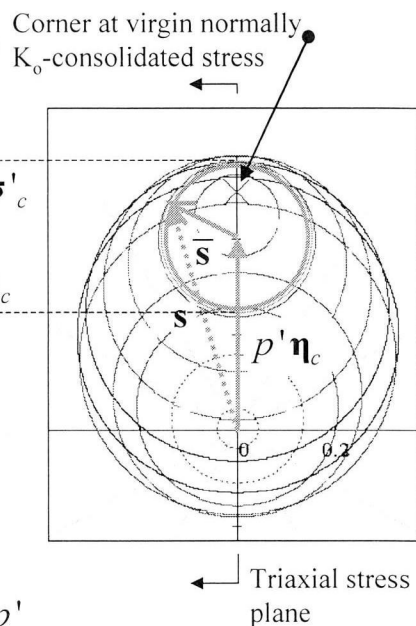
Figure 9: Yield surface on meridional plane

Figure 10: Yield surface on deviatoric plane

References

1) Sekiguchi, H. & Ohta, H., Induced anisotropy and time dependency in clays, 9th ICSMFE, Tokyo, Constitutive equations of Soils, pp.229-238, 1977

2) Britto, A.M. & Gunn, M.J., "Critical state soil mechanics via finite elements", Chichester: Ellis Horwood LTD., 1987

3) Gens, A. & Potts, D.M., "Critical state models in computational geomechanics", *Eng. Comput. 5*, pp.178-197, 1988

4) Roscoe, K.H., Schofield, A.N. & Thurairajah, A., "Yielding of clays in states wetter than critical", *Géotechnique 13(3)*, pp. 211-240, 1963

5) Zienkiewics, O.C. & Pande, G.N., "Some useful forms of isotropic yield surfaces for soil and rock mechanics", in Finite elements in Geomechanics (ed. G. Gudehus), pp.171-190, Wiley, Chichester, 1977

6) Rosco, K.H. & Burland, J.B., "On the generalized stress-strain behavior of 'wet' clay, in J.Heymand & F.A. Leckie (eds.), *Engineering plasticity*, Cambridge University Press, pp. 535-609, 1968

7) Koiter, W.T., Stress-strain relations, uniqueness and variational theorems for elastic-plastic materials with a singular yield surface, *Quart. Appl. Math. (11)*, pp. 350-54, 1953

8) Rudnicki, J.W. & Rice, J.R., "Conditions for the localization of deformation in pressure-sensitive dilatant materials", *J. Mech. Phys. Solids 23*, pp.371-394, 1975

9) Christoffersen, J. & Hutchinson, J.W., "A class of phenomenological corner theories", *J. Mech. Phys. Solids 27*, pp.465-487, 1979

10) Simo, J.C., Kennedy, J.G. & Govindjee, S., Non-smooth multisurface plasticity and viscoplasticity. Loading/unloading conditions and numerical algorithms, *Int. J. Numer. Methods Engrg. 26*, pp.2161-2185, 1988

11) Pipatpongsa, T., Ohta, H., Kobayashi, I. & Iizuka, A., Associated plastic flow at the intersection corner of plastic potential functions in soil mechanics, *Proc. of 36th Japanese Nat. Conf. on Geotech. Engrg,* pp.935-936, 2001

12) Pipatpongsa, T., Kobayashi, I., Ohta, H., & Iizuka, A., The vertex singularity in the Sekiguchi-Ohta model, *56th JSCE Annual Meeting*, in press, 2001

13) Pipatpongsa, T., Ohta, H., Kobayashi, I. & Iizuka, A., Dependence of K_o-value on effective internal friction angle in regard to the Sekiguchi-Ohta model, *Proc. of 36th Japanese Nat. Conf. on Geotech. Engrg,* pp.936-937, 2001

14) Pipatpongsa, T., Ohta, H., Kobayashi, I. & Iizuka, A., Integration algorithms for soil constitutive equations with a singular hardening vertex, *3rd Inter. Summer Sym.*, JSCE, pp.201-204, 2001

15) Iizuka, A. & Ohta, H., "A determination procedure of input parameters in elasto-viscoplastic finite element analysis", *SOILS and FOUNDATIONS 27(3)*, pp.71-87, 1987